Scanning Microscopy

Volume 1 | Number 4 Article 17

8-25-1987

Image Analysis and X-Ray Microanalysis in Cytochemistry

W. C. de Bruijn
Erasmus University

H. K. Koerten
Laboratory for Electron Microscopy

M. I. Cleton-Soeteman
University of Utrecht

C. J. G. Blok-van Hoek
Tracor Europe B.V.

Scanning Microscopy, Vol. 1, No. 4, 1987 (Pages 1651-1667) 0891-7035/87$3.00+.00
Scanning Microscopy International, Chicago (AMF O'Hare), IL 60666 USA

IMAGE ANALYSIS AND X-RAY MICROANALYSIS IN CYTOCHEMISTRY

W.C. de Bruijn*, H.K. Koerten**
M.I. Cleton-Soeteman*** and C.J.G. Blok-van Hoek****

Clinical Pathological Institute, A.E.M.-unit, Erasmus University, K 902, P.O.Box 1738, 3000 DR, Rotterdam and Analytical Electron Microscopy, Lab. for Electron Microscopy, R.U.L. Rijnsburgerweg 10, 2333 AA, Leiden
** Lab. for Electron Microscopy, R.U.L., Leiden
***Pathological Laboratory, University of Utrecht
****Tracor Europe B.V., Bilthoven, The Netherlands.

(Received for publication September 12, 1986, and in revised form August 25, 1987)

Abstract

When cytochemical reaction products are homogeneously distributed within an organelle, point analyses suffice for the quantitative approach. However, quantitative analysis becomes tedious, when the elements in the reaction product are inhomogeneously distributed. Problems arise when elements from two reaction products have to be related to each other, or to endogenous cytological products (ferritin, haemosiderin, calcium, electron dense markers), either topographically or in concentration. When analyzing inhomogeneous/heteromorphical reaction product-containing organelles special attention has to be paid to measure and relate both volume and concentration. In this paper a relative simple structure (eosinophil granules) is chosen to demonstrate that the acquisition of the requested morphometrical plus chemical information and their integration is possible. The following points will be covered to acquire the morphometrical and chemical information:
a). How to estimate the total cell cross-sectioned area. b). How to estimate the total cross-sectioned area of all reaction product-containing particles inside that cell. The ratio of these two areas will provide the requested information about the particle volume fraction. By using the X-ray detector in addition: c). How to acquire the chemical information at the requested resolution, within a reasonable total acquisition time d). How to integrate the morphometrical and chemical data per organelle, by matrix analysis in a reduced scan area. e). How to acquire quantitative chemical information, by the use of cross-sectioned standards. f). How to make this acquisition method independent from changes in the instrumental conditions during the acquisition.

Key words: Image analysis, X-ray microanalysis, morphometry, cytochemistry, signal integration, ultrathin sections, Bio-standards.

*Address for correspondence:
W.C. de Bruijn,
Laboratory for Electron Microscopy, Rijnsburgerweg 10, 2333 AA, Leiden, The Netherlands.
Phone no: 31.71.276466.

Introduction

The combination of either a scanning or transmission electron microscope and an X-ray microanalyzer allows the investigation of chemical elements present in morphologically defined structures in cells and tissues. In histo- or cytochemistry emphasis is placed on the chemical detection of (rest) activity. By the application of a cytochemical reaction the activity present in the cell or tissue is converted in a (mostly electron dense) reaction product. The attached X-ray microanalyzer allows the investigation of the obtained reaction product, either qualitatively for identification, semi-quantitatively (to establish the elemental ratio in it) or quantitatively.

The goal in histo- and cytochemistry is to acquire chemical information about the nature and activity of mostly chemically preserved (= aldehyde-fixed) tissue. Cytochemistry can be defined as: the aim to identify - in a section - the nature of cell structures and their activities, by the introduction of chemical reactions. The chemical reaction is considered successful when the reaction product can be related to a cytological item identified by its morphology.

In light microscopy, morphological contrast can easily be combined with absorption or emission types of colour contrast for the visualization of the reaction product. In electron microscopy, electron scattering was until recently the only way to visualize cytochemical activity. The "presence" of an electron-dense reaction product in a morphologically identified structure had to be related to its "absence" in the non-treated or inhibited control material. Application of X-ray microanalysis allows the differentiation of electron scattering produced by different elements, e.g. separating the elements from cytochemical reaction products from each other or from those visualizing the cellular morphology. Moreover, the obtained metal precipitates or complexes could be quantified, both chemically and/or morphologically.

The conventional transmission electron microscope equipped with an X-ray microanalyzer allows a combination of high morphological

resolution (in the order of 10-20 nm) with a fairly high accuracy of localization of the chemical elements (in the order of 50-100 nm) and rather high sensitivity (> 0.5% local concentration) of elements with a Z-number over 11 (=Na).

The conventional scanning electron microscope (with a secondary and/or backscattered-electron detector and an X-ray analyzer allows, e.g., the analysis of cells from suspensions or tissue cultures, though at a different level of resolution. This type of instrument will be indicated as SEM*.

In the scanning transmission electron microscope (=STEM*) the specimen is scanned by a narrow beam and the image is formed by transmitted electrons. The scanning feature provides an easy way to digitize the image and thereby the possibility to perform image analysis, when the image can be scanned with a matrix of points at equidistance. To acquire both the morphological information, from the electron detector and the chemical information, (from the X-ray detector), the two information streams have to be integrated per matrix point (pixel point). This type of instrument will be indicated as STEM**. In Fig. 1 such an electron microscope is shown schematically.

In most cases, the acquisition and integration of the images have been performed by an operator. However, such a microscope also allows automated analysis, provided that the analyzed structures have sufficient (either chemical or morphological) criteria for recognition by a computer pattern recognition program [1].

In some STEM-type instruments, chemical analysis is not performed by X-ray analysis, but by electron energy loss analysis (30, 32, 52). In such instruments the electrons which have lost energy as a consequence of their interaction with the specimen, are passed through a spectrometer which separates the electron population according to their energy.

With such electron energy loss populations, images can be obtained, which can be related to chemical elements. Such elemental images can be compared with other electron energy loss images, with the elastically scattered or with zero-loss electron images. Investigations by electron probe X-ray microanalysis (EPMA) of endogenous elements by cryoprocedures are excluded from this paper, the reader is referred to reviews dealing with this specific subject [33, 36, 74]. Three-dimensional reconstruction of biological macromolecules [48] is also not included in this paper.

Cytochemical reactions are generally carried out on aldehyde-fixed tissue, though frozen material can also be used for this purpose. In the early days of cytochemistry McGee-Russell and de Bruijn [47] formulated a series of considerations with respect to the aspect of "absence and presence" of cytochemical activity, which still are valid (Table 1).

Here we will not discuss in detail various cytochemical reactions that can be performed to obtain information on the chemical nature of cell organelles and components. A discussion on precipitate formation, inward and outward diffusion, etc. [14, 15, 29] is also outside the scope of this paper. We will simply assume that the chemical reaction results in an electron dense reaction product of which it is desirable to obtain its concentration and volume.

For the visualization of organelles to which the activity is related, osmium tetroxide is mostly used. However, conditions for X-ray microanalysis require the removal of the objective aperture and the use of unstained sections. Cytochemical investigations have been undertaken to increase, in a controllable way, the original osmium contrast in cell membranes and/or glycogen [3, 20, 21, 23, 56, 67]. In addition such investigations contribute to discussions about the way in which osmium tetroxide cytochemically reacts with endogenous cellular structures [7, 71].

The main goal of this paper will be to demonstrate what information can be collected from in situ analysis of ultrathin sections with a chemical element-containing reaction product in an organelle. When the organelles are subject to cellular processes that induce "shape changes" in these organelles or changes in their cytological activity, these changes can be:
1). changes in the volume of the organelles, or
2). changes in the concentration of the cytochemically detected activity. Stereologically related morphometrical methods can give information about the first point. Potentially the STEM** instrument [= with computer-assisted integrated chemical (X-ray) plus morphological (electron) image analysis] allows the additional investigation of a second aspect: the elemental concentration(s).

This paper will be restricted to the acquisition of the morphometrical and chemical data, and the integration of the latter in the former. The reader is referred to results published elsewhere [12, 25, 26], dealing with material, in which several elements (endogenous iron and cerium phosphate from the cytochemical acid phosphatase reaction) are integrated with morphometrical data. Moreover, changes in both sets of data are compared between, pathological human liver material obtained before and after phlebotomy treatment.

Materials and Methods

Our basic instrument is a Philips EM 400 transmission electron microscope equipped with a scanning transmission and a primary backscattered electron detector. In this study only the primary backscattered annular detector was used. A Tracor Northern X-ray microanalytical system is connected to this microscope. For digital beam control, a TN 1310 unit is added. The Tracor Northern Image Processing Program (IPP) was modified to allow the scanning of only part of the normal field (Reduced scan program) [22]. Details of this modification are available, either from the authors or through Tracor Europe, The Netherlands. (Mrs. Blok-van Hoek). The system geometry is described elsewhere [25]. The present results were obtained with a LaB_6 source installed. The beam intensity, measured on the thick

insulated platinum condenser-2 aperture (cylindrical hole diameter= 150 μm) is related to the beam intensity at the specimen plane, but not measured at that plane.

The ultrathin unstained sections are from a cell population from a mouse peritoneal cavity. In this population eosinophil granulocytes are present. The aldehyde-fixed population is treated with a peroxidase reaction with diaminobenzidine (DAB). The poly-DAB formed in the eosinophil granules is visualized by a reaction with H_2PtCl_6 as described elsewhere [27]. The ultrathin sections were collected on 70 mesh copper grids covered with a carbon coated Formvar film. The grids were placed in a beryllium low-background holder. The digital beam control (TN 1310 unit) allows the analysis of areas of the ultrathin section by a matrix of pixel points at equidistances from 16 x 16 to 1024 x 1024. The reduced scan program allows one to direct that matrix of pixel points to specific sites, scanning only a fraction of the total screen area, as in cytochemically treated specimens only particular parts of the cell contain the reaction product. The other features shown in the Results, are related to resolution and dwell time per point. In the present program the acquisition of the electron image is carried out separately from the acquisition of the (maximally four) elemental maps. This carries the risk that, between the two acquisitions, specimen drift has changed the relative positions of the electron image and elemental maps.

The image data acquired at the pixel points, and their relative position in the matrix, are stored on disk. They can be reentered into the computer, and subjected to mathematical treatment. The figures can be printed by the printer/-plotter in such a way that the data are positioned on the paper in the matrix in which they were acquired. This makes the printed "image" resemble the original image on the screen [see Figs. 11, 13 and 14, 15]. This outprint of figures is called array. In arrays that contain two populations of data (cell in epon surroundings, granule in surrounding cytoplasm), a threshold can be introduced, which creates a second so-called overlay image. This overlay image differentiates (in the original array of figures) two sub-populations, one containing the figures above the threshold [called "inside" or I.P.] and one below [called "outside" or O.P.]. In the printed array these populations are separated, by lines drawn between the figures in the array.

In our present print program some relevant results are printed on top of the acquired array-outprints e.g.: total area, number of pixel points in the sub-populations "inside" and "outside", the mean plus standard deviation of the figures in these sub-populations, and whether these values are significantly different. The calculated value for the "inside" part of the image is converted into counts per point, per second, per nm^2. Other relevant information, e.g.the value: mean plus two times the standard deviation is also calculated and printed. This value is used in the objective determination of

X-ray = chemical information | electrons = morphological information

ANALYTICAL ELECTRON MICROSCOPY

X-ray detectors | electron detectors

T/N 2000 | STEM-unit

micrographs
+/-
spectra/outprint

T/N 1310 | TN 1310

ANALYTICAL RESULTS
MORPHOMETRICAL RESULTS
INTEGRATED RESULTS

Fig. 1. Schematic overview of an electron microscope in which both the morphometrical and chemical (X-ray) information can be combined and integrated into one set of integrated information

thresholds [42].

Another feature of the program is that, prior to the acquisition of the elemental intensities in the reduced scan area, a line-scan is acquired in the middle of the area to be analyzed for each element requested. This feature allows the adaptation of the beam intensity or the dwell time to a maximal net-intensity value of 256.

For the determination of elemental concentrations, ultrathin standards of known composition are used [11, 58 - 61]. Several types of standards have been developed, see, e.g. recent reviews collected by Roomans and Shelburne [61]. We prefer the Chelex^{100} or AGMP1 (ion-exchange-resin-based) Bio-standards (BioRad / Polaron) developed in our laboratory [18, 19, 22, 24, 26] as these can be co-embedded with the tissue containing the unknown elemental concentration. These standards have rather high concentrations of a variety of elements, like in cytochemical precipitates. In addition, the cross-sectioned ion-exchange resin material can be conveniently used to adjust the instrumental conditions prior to analysis of the unknown. [for details see 12, 25, 26, 66].

Results

The electron image information. The electron dense platinum-containing eosinophil granules are taken as an example for morphometrical analysis. The CTEM-image is shown in Fig. 2. The S(T)EM image is used to obtain the morphometrical information: (a). the area occupied by the cross-sectioned cell, and (b). the area within that cross-section occupied by the items of interest (= granules). The granules are more electron dense than the cytoplasm and the surrounding platinum-free embedding medium (Figs. 3 and 4). The procedure to acquire the morphometrical information is illustrated in Figs. 5-13. On the S(T)EM**-screen, a single cell is surrounded by a reduced scan frame (white lines in Fig. 3) and the area enclosed is analyzed by a matrix of

Table 1

CONSIDERATIONS IN CYTOCHEMISTRY

1. How much of the substance of interest was present in the object in life?
2. How much of this substance was lost or modified during the steps preceding the moment chosen to perform the reaction to detect its presence or activity or both, by an immuno- or cytochemical reaction?
3. Are chemical reactions available which form stable (electron scattering) reaction products with specific ligands (SH, COOH, NH_2, NH, PO_4) of the structures to detect?
4. Are such reactions applicable at the chosen moment?
5. If reactions are applicable successfully, what is the stability of the reaction product, and how much is sacrificed in subsequent steps of the procedure?
6. How much stable reaction product is formed in the object, and how much in its immediate surroundings (what is the acquired selectivity?).

256 x 256 pixel points. In Fig. 5 the electron-detector derived grey-level information of such a reduced scan is shown. The grey-level values between 0-256 counts per point, are converted to 16 coloured classes, black for the grey-level values between 1-16, white for those between 240-256 electron counts per point, per dwell time (= 4095 µsecs). The frequency histogram of that image is shown in Fig. 6. In that frequency histogram three (Gaussian-shaped) populations of grey-level values are present, viz. embedding medium surrounding the cell, at the lower end of the scale at the left side, the cytoplasm and the granules. To separate the three populations, the grey-level value closest to the cross-over of two Gaussian curves (e.g. those of the embedding medium and the cytoplasm) can be found, either visually by moving the cursor through the histogram, or on the basis of the mean value plus two (or three) times the standard deviation. When the cursor is placed at that position the (16-coloured) grey-level value frequency histogram can be manipulated, viz. one colour can be given to the part below the threshold, whereas the remaining grey-level values above can be redivided into 16 multi- coloured classes (Figs. 7 and 9).

Alternatively the histogram and hence the image can be made binary, viz. one colour below and one colour above the threshold value chosen (Fig. 8). This binary image can be compared with the original image to judge the correctness of the conversion. In the (binary) histogram the number of pixel points inside [I.P.], or outside [O.P.], the cell is given as a percentage of the total number of pixel points present (Fig. 9; 0-114 = epon = 25.25%). As the total area of the analyzed matrix is known, the cellular cross-sectioned area can be calculated. A similar procedure can be carried out for the threshold between the cytoplasm and the cross-sectioned granules (Fig. 10). The quotient of the particle area and the cellular area is the area fraction, which stereologically is related to the volume fraction of the particles within the cell volume, provided sufficient cross-sections can be measured in an identical way. In this way changes in either fraction can be monitored.

X-ray information. At this stage two types of X-ray information can be integrated with the morphometrical data. When the elemental distribution over the item is homogeneous, point analyses can be performed: (a) to discriminate chemically different particles with the same grey-level value, or, (b) to acquire quantitative chemical information. The discrimination can be performed at three levels of automation: 1) by hand, 2) semi-automatically, by localizing points inside the particles followed by point analyses performed automatically at the registered points, or 3) automatically, in our case with the Tracor Northern particle recognition program, PRC, that locates the centers of gravity of the particles and subsequently performs a point analysis [see for details 46, 54, 68]. Quantitative chemical data can be obtained by comparing, in turn, point analyses over a (cross-sectioned) standard with the items of interest, (under the same instrumental conditions).

The X-ray elemental net-intensity images. When elements are inhomogeneously distributed over particles, or the localization of more than one element has to be compared with and related to other elements, X-ray elemental net-intensity distribution images have to be acquired, in the following way:

Reduced scan program. On the S(T)EM**-screen the scan frame is directed towards a single particle to be analyzed, and reduced to fit it (white lines in Fig. 4) and elemental (X-ray) and electron information can be acquired simultaneously, for a range of 16 x 16 to 64 x 64 pixel points per reduced scan frame. The relation between the total acquisition time and the scan reduction is shown in Table 2.

Net-intensity values. To acquire net-intensity values a point analysis is performed on reaction product, to instruct the computer which parts of the spectrum contain the requested regions. In the spectrum (400 eV wide) main regions and several satellite regions are introduced. For each main elemental region selected (= peak plus background = P), a satellite region, representing the continuum under the peak (b), is installed which is subtracted on-line (= P-b). This SRS-method (= single region subtraction), has been described elsewhere [25, 26]. Main regions can also be selected in peak-free continuum portions. By subtracting virtually empty regions as a satellite region from peak-free continuum regions, X-ray continuum maps can be made, for mass distribution ($b-b_0$). Similarly, a satellite region can be subtracted from a continuum region to obtain extraneous-background corrected continuum values ($b-b_e$). At this moment the program is unable to calculate which portion of the peak-free continuum collected in the satellite region originates from extraneous background sources [see also Discussion with Reviewers]. A maximum of four main regions can be acquired at the same

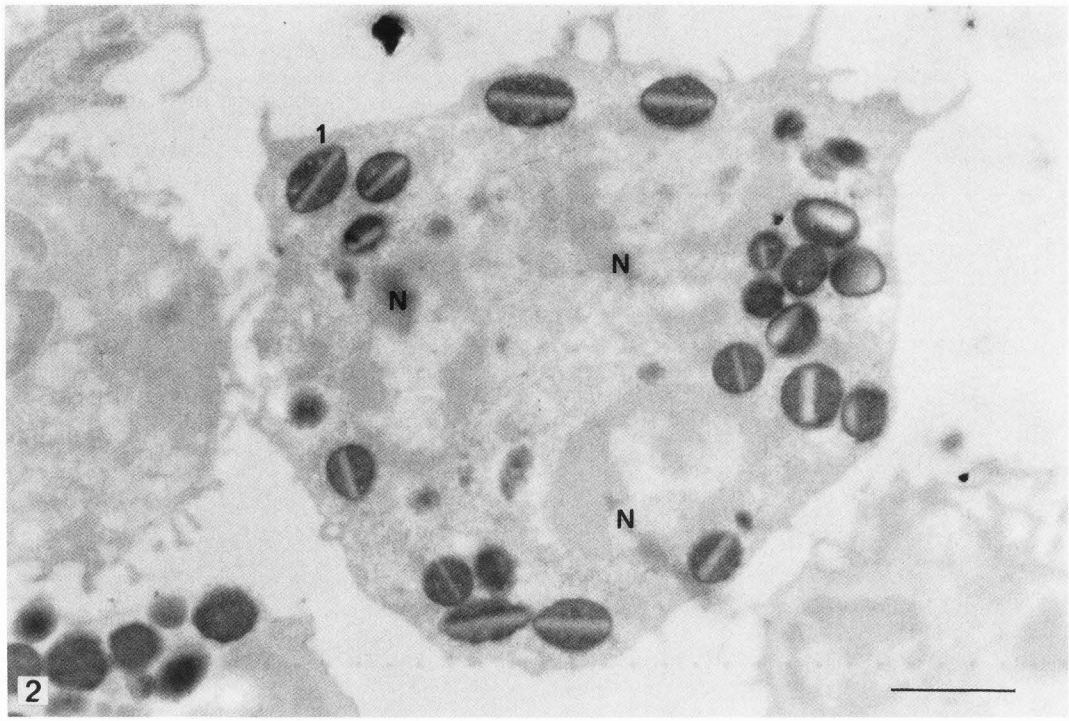

Fig. 2. CTEM-image of an eosinophil granulocyte in which the peroxidase activity located in the coffee-bean-shaped granules, is selectively visualized by a reaction with H_2PtCl_6 at pH = 0.5 at room temperature. No postfixation is applied in this case. Most of the contrast is present in the granules, though the chromatin in the nuclei has also acquired electron scattering capacity (N). One granule (1) is indicated. This granule will be analyzed later in detail. CTEM, 80 keV. Bar = 1 μm.

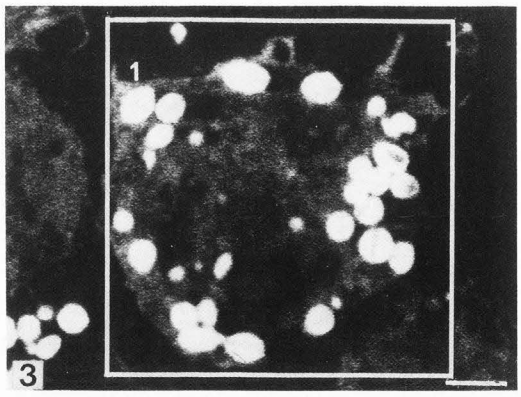

Fig. 3. STEM-image of the same cell as shown in Fig. 2, the position of the reduced scan area is simulated here by the white lines, giving about the same position the reduced scan had taken in reality. The contrast is manipulated to differentiate the electron scattering capacity of the cell plus granules from the surrounding epon. STEM, 80 keV. Bar = 1 μm.

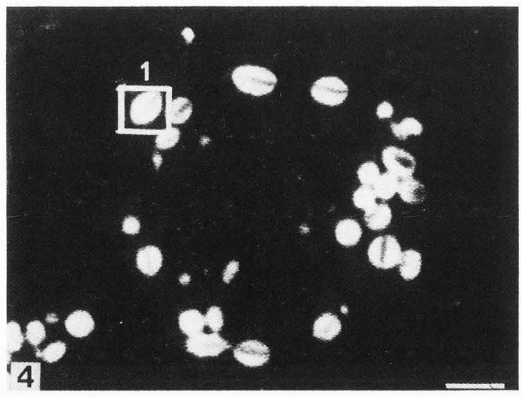

Fig. 4. Same STEM-image as shown in Fig. 3, however, the contrast is manipulated such that the electron scattering capacity is restricted to visualize the granules, containing the highest amount of platinum. The reduced scan applied around one granule (1) is again simulated by the white square. this granule, will be analyzed later (see Figs. 14 and 15).
Figs. 5 - 13: see colour plate on page 1667.

Table 2

INTER PIXEL DISTANCE IN NM AT VARIOUS MATRICES
(initial STEM**-screen magnification = 12.500 x)

Reduced scan in mm	Total area L^2sp.	256x256	32x32	16x16	Final magnification*
90x90	52 μm^2	28 nm	225 nm	450 nm	12,500
40x40	10 μm^2	12 nm	100 nm	200 nm	28,125
20x20	2.6 μm^2	1.6 nm	50 nm	100 nm	56,250
Total pixel points		65536	1024	256	
Total acquisition time is at:					
dwell time/point 1 second		18.2 hr	17 min	4.3 min	
.5 second		9.1 hr	8.5 min	2.2 min	

*: Final magnification on the colour screen 125/90 x this value calculated for the STEM-screen

run. The electron distribution image over the same reduced scan area can be acquired before and/or after the actual X-ray analysis, to monitor specimen drift or to relate the X-ray to the electron information.

Dwell time per pixel point. A line-scan is made across the middle of the reduced scan area, prior to the actual analysis, to determine the dwell time per pixel point. The result of that line analysis of 16 points (or 32 or 64) is given in a graph on the screen for all four main regions. Since the storage capacity of the information per point is only 256 bytes deep, the maximum intensity values have to be kept below 256 counts per point, by reducing the dwell time. Then the grey-level (Figs. 11 and 12) or X-ray net-intensity information (Fig. 13) can be acquired simultaneously. The threshold can be set, to separate the cytoplasm from the granules by finding the cross-over in the, now two (X-ray net-intensity, or electron grey-value) populations in the frequency histogram of the 256 pixel points (Fig. 12).

Integration of the signals. The digitized reduced scan images (Figs. 11 and 13) can be printed as an array of figures, maintaining the relative position of each pixel point in the selected matrix (16 x 16 to 64 x 64), as shown in Figs. 14 and 15. The arrays can be printed with or without a threshold value installed. When a threshold value is introduced, the program prints the original array and includes bars between the figures that separate the values over the threshold from those under. The number of pixels within each sub-population (viz. "inside" and "outside") are printed and the area occupied by the "inside" pixel points calculated. The mean values and standard deviations of the pixels "inside" and "outside" are calculated and printed in the top-legend (Figs. 14-15). In addition it is indicated whether the two populations are significantly different.

As relevant information has been introduced into the computer, (e.g. magnification, spot size and dwell time) several data are directly calculated and printed: the interpixel distance, the total area of the matrix and of the "inside" (I.P.) particle area. The I.P.-area is compared to the number of I.P. pixel points times the spot area. This quotient, the analyzed area, determines the degree the particle is covered by spots used. The figure has to come close to 100%. The acquired X-ray elemental mean net-intensity value from inside the particle is converted into: counts/point/sec./nm^2). Similarly, the standard deviation is expressed in c/p/s/nm^2 plus as a percentage of the mean (= C.V.).

By defaulting the original image, the program prints the location of the separation lines, in relative position to the total array. This can be used to correlate topographically the elemental location in multi-elemental particles in one picture [see Figs. 15-17 in 26 and Figs. 4 and 9-12 in 12]. In the same way a boundary selected in e.g., the electron array can be superimposed over either of the elemental net-intensity arrays acquired (Fig. 16), or the other way around. Also boundaries of two elemental arrays can be superimposed. Irrespective which boundary is chosen, the program performs the same type of calculations from the data present in the original image array, within the superimposed delineation. When no threshold is introduced, the same calculations are performed for the whole array, viz. no "inside" points present (Fig. 17).

The calculated information: mean of the cytoplasmic values plus two (or three) times the standard deviation gives an alternative for the objective determination of the threshold value between cytoplasm and granules (Fig. 17, mean + 2 x St. Dev. = 17 c/p; installed in Fig. 15 = 20 c/p).

Provided the cross-sectioned granule is completely covered by an interconnecting set of spots, the mean net-intensity values represent the exact estimate of the elemental concentration and not a sample out of it. Moreover, accurate morphometrical data are obtained either about the elemental, or about the grey level distribution.

Semi-automatic reduced scan analyses. Once the conditions for the acquisition of the reduced scan analyses of the items of interest (eosinophil granules) are established, the elemental concentration in, plus the area occupied by all particles within one cell can be determined. As mentioned before three levels of automation can be chosen. We preferred the semi-automatic analyses as a good first step, which is performed in the following way: In the binary 256 x 256 electron image of the granule-containing cell, the x/y-coordinates of the particles are introduced in the program. In that way all particles can be included and those not wanted excluded. Subsequently the size of the

```
ORIGINAL IMAGE:VIDEO
OVERLAY IMAGE:VIDEO     OVERLAY THRESHOLD:166
MAGNIFICATION:   168421   TOTAL AREA:    550842 NM**2
LABEL:12-8-85*V16*AC GRAN 1

NUMBER OF POINTS(I P):110      NUMBER OF POINTS(O P):146
MEAN (I P):194.69 C/P          MEAN (O P):122.95 C/P
S. DEVIATION (I P): 17.47 C/P  S. DEVIATION (O P): 18.78 C/P
MEAN+2S.D.(I P):  229.65 C/P   MEAN+2S.D.(O P):  160.52 C/P
DEGREES OF FREEDOM: 254        T-VALUE: 71.74  P < 0.05
DWELL-TIME/POINT:     4095  USEC.
SPOTAREA:   1963 NM**2    ANALYZED AREA 91.75 %
INTER PIXEL DISTANCE:   46 NM  AREA(I P):    236690 NM**2
[VIDEO]=  2.42E+01 C/P/S/NM**2
[S. DEVIATION]=  2.17E+00 C/P/S/NM**2  C.V.=  8.97 %

 131 126 114 109 119 109 112 112 122 111 107 103 115 125 118 115
 114 124 114 120 125 119 102 110 123 127 129 131 126 118 117 114
 117 123 138 131 118 106 122 133 137 153 162 177 163 139 109 106
 127 119 123 113 121 142 156 175 182 189 189 169 170 166 133  97
 124 110 120 131 158 180 183 200 208 183 184 175 172 174 150  96
 120 118 117 141 185 226 221 226 207 192 166 173 176 185 159 103
 117 129 137 181 227 219 229 224 196 187 159 177 205 212 172 104
 110 109 151 219 238 227 231 211 184 165 187 197 198 221 161 115
  95 104 152 219 226 225 200 192 159 170 198 200 199 199 163 136
  81 101 168 200 212 209 198 185 177 203 198 205 203 185 156 130
  85 109 172 198 207 184 188 180 190 202 211 205 199 145 132 126
  86 106 189 221 191 183 180 181 211 202 208 187 173 128 120 127
  98 101 164 216 194 182 190 194 207 194 180 187 138 102 104 123
  93 112 141 189 193 196 195 203 192 171 151 124 111 101 116 121
  99 107 127 142 157 179 170 172 151 146 119 109 109 118 105 119
 121 119 108 113 128 136 124 127 126 123 121 116 106 111 119 119
```

14

Fig. 14 Outprint of the digitalized electron image of Fig. 11 acquired at 16 x 16 pixel points. The grey values are printed within the matrix in which they were acquired. The threshold value (166 c/p/s) separates the granule from the cytoplasm in the printed array by vertical and horizontal lines. In the top-legend of the outprint several calculations, performed by the program can be found.

```
ORIGINAL IMAGE:XRAY PT
OVERLAY IMAGE:XRAY PT     OVERLAY THRESHOLD: 20
MAGNIFICATION:    102885   TOTAL AREA:    1476100 NM**2
LABEL:12-8-85*X16*ACID GRAN 1

NUMBER OF POINTS(I P):102      NUMBER OF POINTS(O P):154
MEAN (I P): 30.33 C/P          MEAN (O P):  9.96 C/P
S. DEVIATION (I P):  6.88 C/P  S. DEVIATION (O P):  5.63 C/P
MEAN+2S.D.(I P):   44.09 C/P   MEAN+2S.D.(O P):   21.22 C/P
DEGREES OF FREEDOM: 254        T-VALUE: 20.37  P < 0.05
DWELL-TIME/POINT:    1000000  USEC.
SPOTAREA:   1963 NM**2    ANALYZED AREA 34.05 %
INTER PIXEL DISTANCE:   75 NM  AREA(I P):    588133 NM**2
[XRAY PT]=  1.54E-02 C/P/S/NM**2
[S. DEVIATION]=  3.50E-03 C/P/S/NM**2  C.V.= 22.68 %

  10  11  11   3  11   1   6   9   8  17   5  13   4   4   7  12
   7  18  10   0  16   9   6   5  12  15  12  18   5   2   6  12
  14   7   4   6  19   7   6   9  19  19  22  24  11  14  10  11
  15  13   3   6  15  13  10  18  26  36  10  17  29  18   7  10
  18   1  14   9   2  13  11  13  27  30  30  20  19  24  27  21
   7  16   3   0  15  28  22  22  38  25  27  27  27  30  14  17
   3   3   6  12   7  18  34  37  19  35  26  42  34  22  30  12
  10  10   6  14  19  24  42  29  37  21  43  21  27  44  29  13
  15   0  11  26  38  50  50  21  31  35  15  26  22  30  18  11
   7   7  18  18  21  30  27  24  29  14  30  34  26  27  34  18
   3   6  10  27  30  36  36  29  26  32  39  42  39  31  26  27
  11   0  11  32  50  41  26  40  19  32  34  41  15   8  34   9
   3  15  19  19  38  26  21  25  35  35  35  25  23   9  15  16
   6  13  23   0  26  24  22  33  26  36  29  27  19   2  10   8
  19   1   7   3  15  18  27  31  23  17   6   5   2   5  14   1
   2  10  10   7   2   3   3  14  18   3  11   8   6   0   2   9
```

15

Fig. 15 Outprint of the Pt net-intensity distribution of granule 1 acquired at 16 x 16 pixel points, shown in Fig. 13. In this case the threshold value, which separates the cytoplasmic Pt net-intensity values from those in the granule, is (20 c/p/s) applied as overlay.

```
ORIGINAL IMAGE:XRAY PT
OVERLAY IMAGE:VIDEO*    OVERLAY THRESHOLD:166
MAGNIFICATION:    102885   TOTAL AREA:    1476100 NM**2
LABEL:12-8-85*X16*ACID GRAN 1

NUMBER OF POINTS(I P):109      NUMBER OF POINTS(O P):147
MEAN (I P): 27.42 C/P          MEAN (O P): 11.12 C/P
S. DEVIATION (I P):  9.38 C/P  S. DEVIATION (O P):  7.82 C/P
MEAN+2S.D.(I P):   46.18 C/P   MEAN+2S.D.(O P):   26.77 C/P
DEGREES OF FREEDOM: 254        T-VALUE: 16.29  P < 0.05
DWELL-TIME/POINT:    1000000  USEC.
SPOTAREA:   1963 NM**2    ANALYZED AREA 34.05 %
INTER PIXEL DISTANCE:   75 NM  AREA(I P):    628495 NM**2
[XRAY PT]=  1.39E-02 C/P/S/NM**2
[S. DEVIATION]=  4.77E-03 C/P/S/NM**2  C.V.= 34.21 %

  10  11  11   3  11   1   6   9   8  17   5  13   4   4   7  12
   7  18  10   0  16   9   6   5  12  15  12  18   5   2   6  12
  14   7   4   6  19   7   6   9  19  19  22  24  11  14  10  11
  15  13   1   6  15  13  10  18  26  36  10  17  31  18   7  10
  18   1  14   9   2  13  11  13  27  30  30  20  19  24  27  21
   7  16   3   0  15  28  22  22  38  25  27  27  27  30  14  17
   3   3   6  12   7  18  34  37  19  35  26  42  34  22  30  12
  10  10   6  14  19  24  42  29  37  21  41  21  27  44  29  13
  15   0  11  26  38  50  50  21  31  35  15  26  22  30  18  11
   7   7  18  18  21  30  27  24  29  14  30  34  26  27  34  18
   3   6  10  27  30  36  38  29  26  32  39  42  39  31  26  27
  11   0  11  32  50  41  26  40  19  32  34  41  15   8  34   9
   3  15  19  19  38  26  23  25  35  35  35  25  23   9  15  16
   6  13  23   0  26  24  22  33  26  36  31  27  19   2  10   8
  19   1   7   3  15  18  27  31  23  17   6   5   2   5  14   1
   2  10  10   7   2   3   3  14  18   3  11   8   6   0   2   9
```

16

Fig. 16 Integrated image. The overlay threshold, that separates in the electron image (Fig. 14) the particle from the cytoplasm is projected over the Pt net-intensity array shown in Fig. 15. The values calculated are from the figures present in the (underlying) Pt net-intensity array.

```
ORIGINAL IMAGE:XRAY PT
OVERLAY IMAGE:XRAY PT     OVERLAY THRESHOLD:  0
MAGNIFICATION:      8058   TOTAL AREA: 240638715 NM**2
LABEL:12-8-85*X16*CYTOPLASM

NUMBER OF POINTS(I P):  0      NUMBER OF POINTS(O P):256
MEAN (I P):  0.00 C/P          MEAN (O P):  6.52 C/P
S. DEVIATION (I P):  0.00 C/P  S. DEVIATION (O P):  5.17 C/P
MEAN+2S.D.(I P):   0.00 C/P    MEAN+2S.D.(O P):   16.88 C/P
DEGREES OF FREEDOM: 254        T-VALUE: -6.52  P > 0.05
DWELL-TIME/POINT:    1000000  USEC.
SPOTAREA:   1963 NM**2    ANALYZED AREA  0.20 %
INTER PIXEL DISTANCE:  969 NM  AREA(I P):          0 NM**2

   0   5  10  14  13  14  15   6   7   8   6   7   7   2  10   5
   1  13  18   0   0  14   3  12   1   9   3  13   6  12  14   7
   7  13  16  16  14   6   4   0   3  14   6  21  19   5  10   9
  11   6   3  10  11   8  15  14  14   6   2   6  14   8   7   8
  19   1  10   0   2   9   2   2   7   8   7   9  11  13  11   3
   3  12   2   2   3   6   7  10   2  12   2   0  10  13  15  10
   6  13  14   2   2   7   7   6   2   2   7  11  10   8   3  15
   7   5   7   3  10   6   6   5   2   0   6   5   2   3   7   5
  18   4   2   0   7   4   2   3   3   3   3   7  19   0  11  19
  10  10   6   2   2   0   2   0   2   3  14  17   7   1  11   0
  10   4  14   4   2   0   7   0  10   1   7   0  18   3  10   2
   6   2   2   0   2   0   3   0   2   0   2  17   3  24  10   1
  11   1  14   8   2   0   2   0   7   0   3   2  10   1   7  11
  11  11  10   6   2   0   2   3   7   2   3   9  18   8   3   2
  14  13  11  10   2   1   2  10   2   0   7   1   7   4   7   3
   6   9  10   8   6   2   2   1   2   0   2   2   7   6   2   2
```

17

Fig. 17 Outprint of a 16 x 16 reduced scan acquisition of the Pt net-intensity values in a particle-free part of cytoplasm. In the outprint the overlay function is dilated by installing threshold value zero. The program then calculates the information contained in the whole array. In this way the threshold value can objectively be determined (=mean plus two times the standard deviation).

reduced scan is adapted to the largest particle of the set and all particles marked are analyzed, and their data stored, in one sequence.

Granule to cytoplasm ratio. The mean granule to cytoplasm ratio can be obtained for both the electron and X-ray image values. In Table 3 such Pt net-intensity granule to cytoplasm ratios are collected for series (n= 20) of eosinophil granules.

Peak to background ratio program. When continuum regions are included in the reduced scan program, peak minus background to background (P-b/b) ratio arrays can be calculated from the stored arrays. In the current ratio program the possibility is introduced to relate mathematically the content of one array to that of another in two ways: a) the two arrays can be divided point by point or b) each value in one array can be divided by the mean value of the other. As a result a quotient array is obtained [see also 12].

The acquisition of a quotient array from a (co-)embedded standard of known C_x results in the value of $K_{cont.}$ for that element, as follows:

$$C_x = \frac{K_{cont.} \cdot I_x}{I_{cont.}} \qquad (1)$$

in which I_x and $I_{cont.}$ are the net-intensity values of the element or the continuum, and $K_{cont.}$ is a proportionality constant. Or, replacing $I_x/I_{cont.}$ by R_x:

$$C_x = K_{cont.} \cdot R_x \qquad (2)$$

In the ratio-program the acquired $K_{cont.}$-factor from the standard can be introduced, hence the quotient array of the unknown becomes directly the concentration array C_x for that element, provided the concentration in the "unknown" does not deviate too much from the concentration in the standard.

To illustrate this point, experiments were performed in which R_x values are monitored in a predictable linear relation to the beam-intensity variation. Fig. 18 (for CTEM/400 nm point analyses), shows that a linear relation is present between the values of the net intensities, calculated for the relation: P-b/I (left side) and P-b/b (right side). The linear regression coefficients of both plots are given in Table 4, from which the $K_{cont.}$ value can be determined for this Bio-standard (≙18.3 % w/w). Similar plots have been obtained for the mean values of 256 points acquired in a 16 x 16 reduced scan area over such cross-sectioned standards.

An additional feature of the ratio program is that from an array the distribution of R_x-values per pixel point can be plotted with increasing magnitude. In Fig. 19 three distribution histograms (256 pixel points) are shown, acquired from a cross-sectioned iron standard and two iron-containing lysosomes, (from material described in [12]). The distribution of the R_x-values in the Bio-standard is rather constant, whereas those from the lysosomes are not, leading to an objective criterion for homogeneous or heterogeneous elemental distribution. By application of the proposed program:

1). The cell cross-section can be estimated.
2). The total cross-sectioned area of reaction-product containing particles inside the cell can be established.
3). The ratio of the two areas represents an unbiased volume estimate of the reaction product in the cell. Volume changes can be determined, provided sufficient cross- sections can be measured in an identical way.
4). Chemical (X-ray) data have been acquired, that topographically can be related to the morphometrical data.
5). Relative concentration values have been established for both the unknown concentration in the reaction product and the co-embedded cross-sectioned standard, in such a way that the measurements are independent from beam intensity and section thickness variations.
6). Correction factors for the extraneous-background contribution and the differences in Z/A^2 between, standard and the unknown can be introduced, though the sub-routines to calculate these corrections still have to be developed.

Discussion

Computer assisted image analysis at the light microscopical level was initially morphometrically oriented [28, 31, 53, see also references in 35]. Gradually also histochemical reaction products were analyzed [5, 43, 44, 45, 73]. The possibility of combining image and elemental analysis in the STEM is due to a convergence of developments in image analysis [8, 10, 34, 50, 51, 55, 62], quantitative X-ray microanalysis [2, 9, 11, 36, 59-61, 65, 69, 70, 72] and high resolution STEM instrumentation [4, 13, 16, 25, 26, 32, 39, 40, 52, 64]. In the past (gross) elemental (X-ray) distribution maps were obtained by using a combination of a rate meter and a so-called "dot-mode" of the STEM*-screen [17, 49]. The disadvantages of this method were successfully alleviated by the introduction of mathematical morphology [63] in the SEM*-image analysis of polished metal surfaces. [41, 54]. The use of pixel masks to locate, measure and quantify continuous matrices of particles (such as in crystalline fractions in composite metals or ceramics) with the assistance of the Kontron/-IBAS-computer is described by Bauer [6]. The computer assisted image analysis in which EELS is used to acquire the chemical information is mostly still qualitative. In the, -in- column-spectrometer of the Castaing/Henry/Ottensmeyer prism/mirror/prism-type, generally the electron spectroscopic images acquired by static beam analysis are digitized afterwards [52]. In the STEM*- instruments with the --out column--, Gatan-type, spectrometers, the focussed electron beam is scanned over the sample area, resulting in an elemental distribution pattern from the spectrometer [13]. As in the early days of the crystal spectrometers for X-ray detection, most of the EELS-detectors are sequential, (one element at a time), whereas background subtraction problems have to be conquered to obtain net-intensity information. (For theoretical aspects of section thickness etc. see [30]). The

Table 3

GRANULES : CYTOPLASM RATIO

	Eosinophil granules		Monocyte granules	
	Reduced scan SRS-method	Point analyses Digital filter	Reduced scan SRS method	Point analyses Digital filter
Pt	2.0	2.8	2.0	2.1

basic problems of computer-assisted image analysis are about the same for all types of analytical instruments. These problems will be explained here with our own system, as described in this paper, as an example.

Image analysis. Images can be considered to be composed of an infinite number of small image fragments. The S(T)EM-image is formed by a series of lines, and each line can be sub-divided in small bits of length or time: image units (= #). Similarly, an image can be subdivided by horizontal and vertical lines drawn at equidistances. At the line intersections (= pixel points) image information can be acquired. Each element of image information collected at the pixel points can be considered to be an image unit #. When the acquired image information can be recorded as a single number, the image can be considered to be digitized. Storing these numbers and their relative positions during acquisition allows image reconstruction. The number of image units, #, needed to adequately reconstruct the total image matrix depends on the resolution one wants to achieve. When the acquired digital information is of "structural origin", (recorded as grey-level values, see Fig. 14) the inter pixel distance (IPD) can replace the term resolution (= minimal distance to be resolved/recorded). For the chemical X-ray information, the acquired figure represents a fractional concentration, which topographically can be related to other concentrations of the same or other elements.

Resolution of the images. In most scanning microscopes the resolution of the screen is 1000 lines per frame height. At a frame height of 90 mm, the vertical line resolution is 90 µm. The relation of the screen resolution to the specimen resolution is given in equation (3):

$$d_{sp} = \frac{d_{sc}}{M \cdot N} \qquad (3)$$

in which d is the distance on the specimen (sp) and d_{sc} = the screen height, M the microscope magnification and N the number of lines per frame height.

When a 90 x 90 mm screen area is covered by 1024 x 1024 pixel points, the same vertical and lateral resolution on the original screen is obtained and hence the interpixel distance on the specimen:

$$IPD_{sp} = d_{sp} = \frac{d_{sc}}{M \cdot N} \qquad (4)$$

in which N is the number of pixel points/line. For CTEM-micrographs, it is required that the minimal diameter (d_{min}) of the image "particle" to be resolved, is 2-5 times (= f, in eq. 5) the "noise particle diameter" (d_{no}) of the film material used for recording:

$$d_{min} = f \cdot \frac{d_{no}}{M} \qquad (5)$$

If we assume that on the STEM**-screen the particle to be resolved, has to be crossed by at least 4 lines and d_{no} = screen resolution (d_{sc}), the relation between (M), the magnification and the (minimal) particle diameter at the specimen plane becomes:

$$d_{min} = \frac{4 \cdot d_{sc}}{M} \qquad (6)$$

At M=12,500, d_{min} is about 28 nm at the specimen plane. A square particle of 28 x 28 nm in the specimen plane is covered by 16 pixel points, a circular particle by about 12 pixel points, each at an equidistance of 7.2 nm (= IPD_{sp} for N = 1024). So:

$$d_{min} = f \cdot IPD_{sp} \qquad (7)$$

When the full (90 x 90 mm) screen is not scanned, the actual length of the reduced line is directly introduced for d_{sc} or a reduction factor F has to be added in the numerator of eq. 4. The IPD_{sp} remains the same when in the denominator of eq. 4, N is multiplied by the same reduction factor.

Interpixel distance, spot size and coverage. Special attention must be paid to the aspect that the whole area/volume of the item is analyzed, by choosing the correct spot size and IPD. (See Figs. 15-16 in ref. [25] and Figs. 9-12 in ref. [12] and Figs. 14-17 in this paper). The section surface, within a scanned square, is covered by an interconnecting, partially overlapping, matrix of spots, when (at M = 12,500 and 1024 x 1024 pixel points) a circular spot of 10nm diameter is used (spot-size = $IPD_{sp} \cdot \sqrt{2}$). When the section thickness is considered, the information comes from a truncated conical volume with a top area of 78.5 nm^2 and a bottom area of unknown diameter, due to (element-dependent) beam-broadening. Therefore, beam-broadening has to be taken into account to determine the correct volume for the calculation of the X-ray (or grey level value) concentration in the cross-sectioned object. This condition of complete coverage of the object's section surface can be considered a prerequisite for a correct chemical resolution. Beam-broadening can be calculated from homogeneously distributed elements in Bio-standards [see for discussion 25, 26]. In our instrument the available (STEM) spot sizes are : 100, 50, 20, 10, 5, 2 nm. By balancing the components of eq. 4, the whole range of spot sizes can be covered. The percentage of the matrix covered by

Table 4

LINEAR REGRESSION LINES CHELEX^{100} + Pt (CTEM)

Element	equation y = a + bx	probability P-b/i
Platinum-Mα	0.14 + 0.65x	0.9939
Platinum-Lα	0.18 + 0.31x	0.9931
Element	**equation**	**probability P-b/b**
Platinum-Mα	-0.16 + 1.95x	0.9983
Platinum-Lα	0.03 + 0.92x	0.9978

the (IP) pixel points of the spot size used plus the IPD_{sp} is printed in the top-legends of the arrays. The degree of beam-broadening is not taken into account. So the %-coverage value does not reach 100% when the spot size is adopted to include beam-broadening.

Total acquisition time in relation to dwell time per pixel point. The main practical reason to propose the reduced scan program was to economize on the acquisition time by eliminating the area not containing relevant cytochemical information. We used the annular detector to image the ultrathin sections. The backscattered electron-detection efficiency of this detector is very high due to the large solid angle of collection and consequently a rather short dwell time per pixel point can be accepted for good statistics. This limits the total acquisition time for the full frame. The X-ray detection efficiency is generally much smaller, whereas the backscattered-electron yield per incident electron is higher than the X-ray yield, so longer dwell times per pixel point are needed for good X-ray acquisition statistics. In Table 2 it is illustrated that X-ray analysis at 1 sec. per pixel point can only be performed within reasonable time in matrices with less pixel points (e.g. in 16 x 16, 32 x 32 or 64 x 64 matrices), without sacrificing resolution.

Subtraction of the continuum portion under the peak. The true continuum part present under the characteristic X-ray signal in the main region has to be subtracted, to obtain net-intensity values [37, 38, 69]. For point analyses, several subtraction methods are known [26, 57]. However, not all methods can be applied here, as in most cases a complete spectrum has to be available and not main and satellite regions, like in this program. We proposed two methods of background subtraction applicable to the on-line method used in the reduced scan analysis: SRS = single region subtraction and DBL = double region subtraction [26]. In practice both methods are joined. For a given elemental peak the continuum under the peak is calculated by the DBL method. Subsequently a single peak-free continuum region is selected in which the value corresponds with that true continuum region calculated, which region then is used in the SRS-method. For the DBL-method, the two chosen continuum regions at either side of the main peak have to be of the same width as the main region (= 400 eV). For the SRS-method there is no need for this, as only the contents of this satellite region to be subtracted is relevant.

Subtraction of the extraneous background. In a similar way the extraneous background contribution to the satellite continuum region can be subtracted. On-line, the satellite region "zero" [see 26] can be moved, so that its contents represents that extraneous background portion.

The conversion factor Kcont.for standard and specimen. The concentration arrays as acquired can correct for possible inaccuracies in section thickness and beam intensity variation [12].

To compare the concentration in the "unknown" with those in the standard Roomans [60] suggested the use of an equation derived from an expression given by Hall [37]:

$$C_{x,sp} = C_{x,st} \cdot \frac{R_{x,sp} \cdot \overline{Z^2/A_{sp}}}{R_{x,st} \cdot \overline{Z^2/A_{st}}} \qquad (8)$$

in which C_x is the mass fraction of element x, Z is the atomic number, A the atomic weight, and Z^2/A the averaged values in the specimen and the standard for all elements present, weighted according to their mass fraction. $R_{x,sp}$ and $R_{x,st}$ are defined as (extraneous background corrected) P-b/b of x in standard and unknown. The $K_{cont.}$-factor includes Z^2/A_{st}. When the concentration in the standard resembles that of the specimen, $Z^2/A_{sp} = Z^2/A_{st}$, hence a correction factor is cancelled out. If this condition does not apply the $k_{cont.}$-factor has to be adopted for the differences between Z^2/A_{sp} and Z^2/A_{st} in the calculation of $C_{x,sp}$. Roomans used a computer program with an iterative method to match this Z^2/A-value with high accuracy [59].

The discussion whether to use the mean background value acquired over all 256 pixel points or to use the background acquired per pixel point has not yet come to a conclusion. When the section has a high number of imperfections (holes, thickness variations) the point/point ratio mode will follow these variations closer than the mean background-mode.

The print program. The reason to develop the print program was to have access to the figures in the array, to perform quantitative calculations.

The information now present in the top-legends of the array-outprints is also valuable without the printed array at the bottom, and the array can easily be eliminated.

Particle to cytoplasm ratio. The possibility to discriminate between a particle and the surrounding cytoplasm is determined by the difference between the elemental concentrations in the two compartments [42]. Our program calculates whether these (mean) values are significantly different. It has been discussed elsewhere [27] that by introducing X-ray microanalysis in

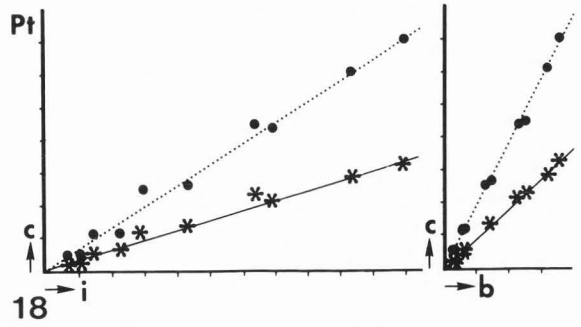

Fig. 18. At the left-hand side, multiple point analyses over a Chelex^{100} maximally-Pt-loaded cross-sectioned Bio-standard, acquired at 80 keV in the CTEM- mode with 400 nm spotsize. All Beam-intensity variations are imposed. Dotted line Pt Ma net- intensities, drawn line, Pt-La--net-intensities. (C = Peak minus background vs. beam intensity). At the right-hand side the same Pt net-intensity values are related to the concomitantly acquired values in a peak-free background region. The regression lines calculated are also given in Table 4.

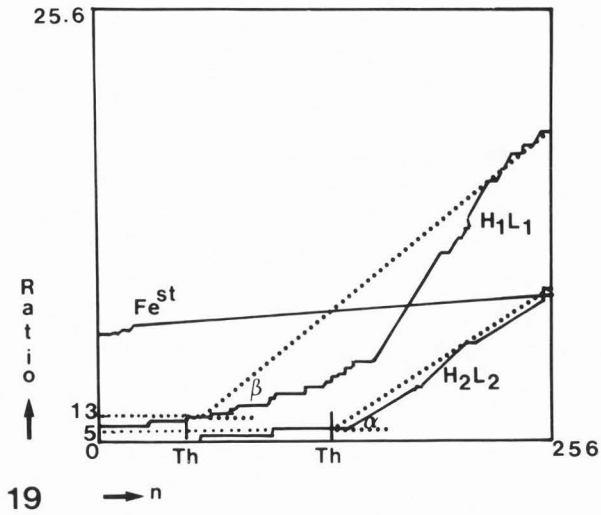

Fig. 19 Compilation of iron mass fractions (P-b/b-ratio) per pixel point (0-256) of two lysosomes, before (= H1L1) and after (H2L2) phlebotomy and the iron-containing Bio-standard (Fe_{st}). The mean values in the cytoplasms (13 and 5) are indicated. The angles between the lowest values over the threshold (Th) and the highest value are indicated for both lysosomes.

quantitative cytochemistry the absence of a (positive) signal implies that the local elemental concentration is below the minimal detectable limit of this analytical instrument. i.e., between 0.04 and 2.5 % w/w. [66]). Contrary to the rather pessimistic view of Shuman et al. [64] our results show that in cytochemistry compositional element mapping can successfully be applied, in spite of a rather low granule to cytoplasm ratio of about two (Table 3).

References

1. Abe T, Marimoto K, Wakabayash, Soezima H. (1980). A fully automatic X-ray microanalyszer. In: Electron Microscopy 1980. P. Brederoo, W. de Priester (eds.) Seventh Europ. Congr. on Electron Microsc. Foundation, Leiden 1980. p. 142.
2. Albert L. (1973). How thin layers and how localized masses can be detected by means of electron probe microanalysis? -A theoretical investigation. Beitr. Elektronenmikroskop. Direktabb. Oberfl. 6, 19-41.
3. Angermüller S, Fahimi HD. (1982). Imidazole buffered osmium tetroxide: an excellent stain for visualization of lipids in transmission electron microscopy. Histochem. J. 14, 823-835.
4. Arsenault AL, Ottensmeyer FP. (1983). Quantitative spatial distribution of calcium, phosphorus and sulfur in calcifying epiphysis by high resolution electron spectroscopic imaging. Proc. Natl. Acad. Sci. USA 80, 1322-1326.
5. Bacsy E. (1982). Enzymatic heterogeneity of adrenalcortical lysosomes: an X-ray microanalytical study. Histochem. J. 14, 99-112.
6. Bauer B, Schwarz H, van Tanh N. (1983). Digital image processing of combined EM and EDX signals. J. Microsc. 130, 325-330.
7. Behrman EJ. (1980). On the oxidation state of osmium in fixed tissues. J. Histochem. Cytochem. 28, 285-286.
8. Boyes ED, Muggridge BJ, Goringe D. (1982). On-line image processing in high resolution electron microscopy. J. Microsc. 127, 321-335.
9. Carlemalm E, Garavito RM, Villiger W. (1982). Resin development for electron microscopy and an analysis of embedding at low temperature. J. Microsc. 126, 123-143.
10. Carlemalm E, Villiger W, Hobot JA, Acetarin JD. (1985) Low temperature embedding with Lowicryl resins: two new formulations and some applications. J. Microsc. 140, 55-63.
11. Chandler JA. (1977). Quantitative X-ray microanalysis. In: X-ray microanalysis in the electron microscope (Practical Methods in E.M.) AM. Glauert, (ed.). North-Holland Publ. Co., Amsterdam, Oxford. p. 490-492.
12. Cleton MI, Roelofs JM, Blok-van Hoek CJG, de Bruijn WC. (1986). Integrated image and X-ray microanalysis of hepatic lysosomes in a patient with idiopathic hemosiderosis before and after treatment by phlebotomy. Scanning Electron Microsc. 1986; III: 999-1006.
13. Colliex C, Jeanguilliaume C, Mory C. (1984). Unconventional modes for STEM imaging of biological structures. J Ultrastruct. Res. 88, 177-206.
14. Cornelisse CJ, van Duijn P. (1973). A new method for the investigation of the kinetics

of the capture reaction in phosphatase cytochemistry. I. Theoretical aspects of the local formation of crystalline precipitates. J. Histochem Cytochem. 21, 607-613.
15. Cornelisse CJ, van Duijn P. (1973). A new method for the investigation of the kinetics of the capture reaction in phosphatase cytochemistry. II. Theoretical and experimental study of phosphate diffusion from thin polyacrylamide films. J. Histochem. Cytochem. 21, 614-620.
16. Crewe AV. (1984). An introduction to the STEM. J. Ultrastr. Res. 88, 94-104.
17. De Bruijn WC, Schellens JPM, van Buitenen JMH, van der Meulen J. (1979). X-ray microanalysis of colloidal-gold labeled lysosomes in rat liver sinusoidal cells after incubation with acid phosphatase activity. Histochemistry 66, 137-148.
18. De Bruijn WC. (1981). Ideal standards for X-ray microanalysis of biological specimens. Scanning Electron Microsc. 1981; II: 357-367.
19. De Bruijn WC. (1981). Ion exchange beads as standards for X-ray microanalysis of biological tissue. Beitr. Elektronemikrosk. Direktabb. Oberfl. 16, 369-372.
20. De Bruijn WC, van Buitenen JMH. (1980). X-ray microanalysis of aldehyde-fixed glycogen contrast - stained by $Os^{VI}.Fe^{II}$ and $Os^{VI}.Ru^{IV}$ complexes. J. Histochem. Cytochem. 28, 1242-1250.
21. De Bruijn WC, van Buitenen JMH. (1981). X-ray microanalysis of non-aldehyde-fixed glycogen contrast - stained by $Os^{VI\,I\,I}O_4$, $Os^{VIII}.Fe^{III}$, or $Os^{VI}.Fe^{II}$ complex in vitro. Histochem. J. 13, 125-136.
22. De Bruijn WC, Zeelen JPh. (1983). Combined image and X-ray microanalysis of biological material. Beitr. Elektronenmikrosk. Direktabb. Oberfl. 16, 385-388.
23. De Bruijn WC, Memelink AA, Riemersma JC. (1984). Cellular membrane contrast and contrast differentiation with osmium triazole and tetrazole complexes. Histochem. J. 16, 37-50.
24. De Bruijn WC. (1984). Standards for quantitative X- ray microanalysis of biological specimens. Les Editions de Physique. Colloque C2, Suppl. 2; Tome 45, Les Editions de Physique.Toulouse, France p. 469-472.
25. De Bruijn WC. (1985). Integration of X-ray microanalysis and morphometry of biological material. Scanning Electron Microsc. 1985; II: 697-712.
26. De Bruijn WC, Cleton MI. (1985). Application of Chelex standard beads in integrated morphometrical and X-ray microanalysis. Scanning Electron Microsc. 1985; II: 715-729.
27. De Bruijn WC, van der Meulen J, Brederoo P, Daems WTh. (1986). Pt-staining of peroxidatic reaction products at the ultrastructural level. Histochemistry, 84, 492-500.
28. Dehoff RT. (1968) Measurements of number and average size in volume In: Quantitative microscopy, Dehoff RT, Rhines FN. (eds.) McGraw Hill, New York, p. 128-148.
29. De Jong ASH, Hak TJ, van Duijn P, Daems WTh. (1978). A new dynamic model system for the study of capture reactions for diffusible compounds in cytochemistry.I. Description of the model with special attention to phosphatase capture in acid phosphatase cytochemistry. J.Histochem.Cytochem. 26, 331-339.
30. Egerton RF. (1981). Alignment and characterization of an electron spectrometer. Ultramicroscopy 6, 93-96.
31. Elias H, Hennig A. (1966). Stereology of the human renal glomerulus. In: Quantitative Methods in Morphology. Weibel ER, Elias H. (eds.) Springer Verlag Berlin, Heidelberg, New York. p. 130-166.
32. Engel A, Reichelt R. (1984). Imaging of biological structures with the scanning transmission electron microscope. J. Ultrastruct. Res. 88 105-120.
33. Frederik PM. (1982). Cryoultramicrotomy - recognition of artifacts. Scanning Electron Microsc. 1982: II; 709- 721.
34. Gravekamp C, Koerten HK, Verwoerd NP, de Bruijn WC, Daems WTh. (1982). Automatic image analysis applied to electron micrographs. Cell Biol. Intern. Rev. 6, 656-657.
35. Gundersen HJG, Jensen EB. (1983). Particle sizes and their distribution from line and point-sampled intercepts. Including graphical unfolding. J. Microsc. 131, 291-310.
36. Hagler HK, Lopez LE, Flores JS, Lundswick RJ, Buja LM. (1983). Standards for quantitative energy dispersive X-ray microanalysis of biological cryosections: validation and application to studies of myocardium. J. Microsc. 131, 221-234.
37. Hall TA. (1971). Microprobe assay of chemical elements, In; Optical Techniques, Vol 1a, 2nd ed. G. Oster (ed.) Academic Press, New York, London. p. 157-275.
38. Hall TA, Clark Anderson H, Appleton T. (1973). The use of thin specimens for X-ray microanalysis in biology. J. Microsc. 99, 177-182.
39. Harauz G, Ottensmeyer FP. (1984 a). Direct three- dimensional reconstruction for macromolecular complexes from electron micrographs. Ultramicroscopy 12, 309-320.
40. Harauz G, Ottensmeyer FP. (1984 b). Nucleosome reconstruction via phosphorus mapping. Science 226, 936- 940.
41. Jeulin D. (1980). Morphological SEM-picture processing. Institute de Recherche de la siderurgie Francaise. IRSID, MESRE 864, France. p. 1-36.
42. Johannsen G, Bille J. (1982). A threshold selection method using information measures. Proc. Int. Conf.Pattern Recognition. Inst. Electrical. Electronic Engineers Inc. Computer Soc. Press. München, Vol. 1 p. 140-142.
43. Kendall MD, Warley A, Morris IW. (1985). Differences in apparent elemental composition of tissues and cells using a fully quantitative X-ray microanalysis system J. Microsc. 138, 35-42.
44. Knoll TF, Brinkley LL, Delp EJ. (1985). Different picture algorithms for the analysis of extracellular components of histological images. J. Histochem Cytochem. 33,

261-267.
45. Lytton DG, Eastgate AR, Ashbolt NJ. (1985). Digital mapping of metal-bearing amobocytes in tissue sections of the Pacific oyster by scanning microphotometry. J. Microsc. 138, 1-14.
46. McCarthy JJ, Fisher RM, Lee, RJ. (1982). Applications of computers in electron microscopy. Ultramicroscopy 8, 351-360.
47. McGee-Russell SM, de Bruijn WC. (1968). Image and Artifact - Comments and experiments on the meaning of the image in the electron microscope. In: Cell Structure and its Interpretation. SM McGee-Russell and KFA Ross (eds.) E. Arnold Ltd. London p. 115-133.
48. Mellema JE. (1980). Computer reconstruction of regular biological objects. In: Topics in Current Physics. PW Hawkes. (ed.) Springer Verlag. Berlin, Heidelberg, New York. p. 89-125.
49. Morgan AJ. (1985). X-ray microanalysis in electron microscopy for biologists. Oxford University Press, Royal Microscopical Society, 1985. p. 30-51.
50. Nawrath N, Serra J. (1979). Quantitative image analysis: Theory and instrumentation. Microscopica Acta 82, 101-128.
51. Niemietz A, Reimer L. (1985). Digital image processing of multiple detector signals in scanning electron microscopy. Ultramicroscopy 16, 161-174.
52. Ottensmeyer, FP. (1984). Electron spectroscopic imaging: parallel energy filtering and microanalysis in the fixed- beam electron microscope. J. Ultrastruct. Res. 88, 121- 134.
53. Peters, JPJ, Rademakers, LHPM, Roelofs JMM, de Jong D, van Unnik JAM. (1984). Distribution of dendritic reticulum cells in follicular lymphoma and reactive hyperplasia. Virchows Arch. (Cell Pathol.) 46, 215-228.
54. Pinxter JFM. (1985) Applications of digital electron beam control - a status report. Optical and electron microscopy 15, 1-5.
55. Reichelt R, Carlemalm E, Villiger W, Engel A. (1985). Concentration determination of embedded biological matter by scanning transmission electron microscopy. Ultramicroscopy 16, 69-80.
56. Riemersma JC, Alsbach EJJ, de Bruijn WC. (1984). Chemical aspects of glycogen contrast staining by potassium osmate. Histochem. J. 16, 123-136.
57. Roomans GM, van Gaal HLM. (1977). Organometallic and organometalloid compounds as standards for microprobe analysis of epoxy resin embedded tissue. J. Microsc. 109, 235-240.
58. Roomans GM, Seveus, LA. (1977). preparation of thin cryosectioned standards for quantitative microprobe analysis. J. Submicr. Cytol. 9, 31-35.
59. Roomans GM. (1979). Quantitative X-ray microanalysis of halogen elements in biological specimens. Histochemistry. 65, 49-58.
60. Roomans GM. (1979). Standards for X-ray microanalysis of biological specimens. Scanning Electron Microsc. 1979: II, 649-657.
61. Roomans GM. (1983). Standards for X-ray microanalysis of biological specimens. In: Basic Methods in Biological X-ray Microanalysis. Roomans GM, Shelburne JD. (eds.). Scanning Electron Microsc. Inc. AMF O'Hare. Il. 60666. p. 251-260.
62. Russ JC, Russ JChr. (1984). Image processing in a general purpose microcomputer. J. Microsc. 135, 89-102.
63. Serra J. (1982). Image analysis and mathematical morphology. Academic Press, London. p. 55-60.
64. Shuman H, Somlyo AV, Somlyo AP. (1976). Quantitative electron probe microanalysis of biological thin sections: Methods and validity. Ultramicroscopy 1, 317-339.
65. Somlyo AP. (1984). Compositional mapping in Biology: X-rays and electrons.J. Ultrastruct. Res. 88, 135-142.
66. Van der Wolk FM, de Bruijn WC. (1984). Ion-exchange beads as standards in ultrathin sectioned biological material. Proc. Dutch Soc. for E.M.. Wageningen. p. 29.
67. Van Emburg P, de Bruijn WC. (1984). Enhanced cellular membrane contrast in a marine alga by osmiumazole complexes. Protoplasma 119, 48-54.
68. Van Noord MJ, van Hoek CJM. (1980) Quantitative X-ray microanalysis of asbestos standards (thin specimens) with various computer programs. Ultramicroscopy 5, 127.
69. Warner RR, Myers MC, Taylor DA. (1985). Inaccuracies with the Hall technique due to continuum variation in the analytical microscope. J. Microsc. 138, 43-52.
70. Werner HW. (1980). Modern methods for thin film and surface analysis In; Electron Microscopy 1980-3, P. Brederoo, W. de Priester (eds.). Seventh Europ. Congr. on Electron Microscopy Foundation, Leiden 1980. p. 200-207.
71. White DL, Mazurkiewicz JE, Barnett RJ. (1979). A chemical mechanism for tissue staining by osmium tetroxide-ferrocyanide mixtures. J. Histochem Cytochem. 27, 1084-1089.
72. Wroblewski J, Roomans GM, Madsen, K, Friberg U. (1984). Effects of growth hormone and insulin on cultured chondrocytes studied by X-ray microanalysis. Proc. Eur. Congr. on Electron Microscopy.(A. Csandy, P. Röhlich, D. Szabo (eds.) Motez Budapest. p. 1723-1724.
73. Yoshioka T, Somlyo AP. (1984). Calcium and magnesium contents and volume of the terminal cisternae in caffeine treated skeletal muscle J. Cell Biol. 99, 558-568.
74. Zierold K, Schäfer D, Pietruschka F. (1984). The elemental distribution in ultrathin cryosections of cultivated fibroblast cells. Histochemistry 80, 333-337.

Discussion with Reviewers

GM Roomans: In Fig. 17, the threshold is set 0; I would think it would be more logical to call all points "in" rather than "out". What happens

if you put the threshold at 256?
Authors: You are right. We just selected one of the two to obtain the results. We had it changed afterwards. Recent changes also include: the possibility to obtain the top legend, without having the array printed, and to have only part of the information (Total area, (IP)-area, mean (IP) values plus (IP) standard deviation).

GM Roomans: The background subtraction method used by the authors is certainly correct with isolated peaks and high P/B values. I have no objections in the context of this paper, but the authors could mention filter methods or even least square fitting methods as further developments.
Authors: We agree, but underline that not all methods can be applied on-line. We can imagine that instruments with a fast array processor connected can be programmed to perform the requested filtering or fittings during the acquisition phase of each point. The crucial point remains whether the reduction of the dwell time per pixel point to about 1 s. gives reliable counts to apply the (basically statistical) methods mentioned. So the question of subtraction or filtering remains. We would like to emphasize that the applied (SRS) substraction method does not exclude the possibility to find a satellite region that contains a value proportional to the value subtracted by the filter method applied on the 100 s. point analysis.

GM Roomans: I would suggest that the extraneous background could be subtracted by the following procedure:
Complete spectra are acquired from each of the structures mapped (specimen, sp), the film (f) covering the grid (but not with embedding plastic) and the naked grid (g). If W denotes the background, and G the net counts of the grid material, the extraneous background is given by:

$$W_e = W_f - (G_{sp} - G_f)\ (W_g/W_{sp}) \qquad (q)$$

(75-77). It is a reasonable assumption that these values are the same for each pixel point of the reduced scan. This means that G_{sp} only needs to be determined once for each structure mapped, W_f and G_f once for each grid, and W_g and G_g once for each experiment. For differences in collection time between the spectrum and pixel point one can correct by:

$$(W_e/W_{sp})\ \text{spectrum} = (W_e/W_{sp})\ \text{pixel point}$$

and either calculate W_e based on W_{sp} for each pixel point or better on the average W_{sp} for all pixel points (W_e will not vary noticeably between pixel points). Then, the correction for W_e simply amounts to subtracting a constant from the obtained background array. Would it be possible to incorporate this procedure in your program?
Authors: The answer to the question is yes. Once a background array is obtained (in our terminology $b\text{-}b_0$) it is clear that a fraction of each pixel point value or the mean value belongs to the extraneous background. The idea is to try to cut off that slice either from each pixel point or from the mean value calculated afterwards. The simplest way to do so was to move the satellite region zero to a point in the spectrum where the contents represented that extraneous background. In that case on-line the $(b\text{-}b_0)$-array would become the $(b\text{-}b_e)$-array, and in the ratio program the R_x-array, would become the R_x -array (= corrected for extraneous background) for both the standard and the "unknown", when the standard and the unknown are in the same section. Now you are pushing the ball one step further, viz. to determine the b_e correctly. This might be the object for a future study (78).

GM Roomans: In the cases such as described in this paper, the changes in Z^2/A_{sp} are mainly determined by changes in the $C_{Pt,sp}$. Hence we can say that by approximation:

$$Z^2/A_{sp} = C_{Pt.sp} \cdot Z^2/A_{Pt} + (1 - C_{Pt,sp}) \cdot Z^2/A_m$$

where Z^2/A_m is the weighted mean value of Z^2/A for the "matrix" (all elements except Pt) in the specimen. $C_{Pt,sp}$ is given as mass fraction. The approximation lies in treating Z^2/A_m as a constant. We can also define a constant $S_{Pt,sp}$ as:

$$S_{Pt,st} = (C_{Pt,st}) / (R_{Pt,st} \cdot Z^2/A_{st}) \qquad (s)$$

By inserting these two equations into equation (8) of the paper, and rearranging the terms, we obtain:

$$C_{Pt,sp} = \frac{S_{Pt,st} \cdot R_{Pt,sp} \cdot Z^2/A_m}{1 + S_{Pt,st} \cdot R_{Pt,sp} (Z^2/A_m - Z^2/A_{Pt})} \qquad (t)$$

(76). Since all terms on the right hand side of this equation, except $R_{Pt,sp}$ are constant, it would be theoretically possible to carry out a simple (non-iterative) calculation on all $R_{Pt,sp}$. Would it be practically possible to incorporate this procedure in your program?
Authors: In this case also, the answer to the question is yes. In the ratio-program converting R_x into C_x, a multiplication factor is required. In our case we suggested to include the $K_{cont.}$-factor, with the restriction that C_{st} and C_{sp} (using your terminology) were about equal. The idea to match these concentrations was originally put forward when introducing the Bio-standards [18, 19, but see also 66 and 78].

Whenever that is not the case, the $K_{cont.}$-factor needs further correction. Equation (s) for $S_{Pt,st}$ can be written in our terminology as $K^*_{cont.}$ whereby $K^*_{cont.} = K_{cont.} / Z^2/A_{st}$. From your eq.(r) we had prepared a nomogram in which values for $C_{Pt,sp}$ ranged from 1 - 50% and the calculated values were used to correct the $K_{cont.}$ or $K^*_{cont.}$-factor. The $Z^2/A_{Pt,st}$ value according to eq. (s) was 10 (taking Z^2/A_m as 3.1).

Your proposal can be rearranged according to the demands of the ratio program according to:

$$C_{Pt,sp} = f_{Pt,sp} \cdot R_{Pt,sp}, \text{ in which}$$

$$f_{Pt,sp} = \frac{K^*_{cont.} \cdot Z^2/A_m}{1 + (K^*_{cont.} \cdot R_{Pt,sp} \cdot Z^2/A_m - Z^2/A_{Pt})}$$

K Zierold: Why do you use the backscattered electron? Is the backscattered electron signal sufficient for studies of ultrathin sections?
Authors: There is not a particular scientific reason. In the first instrument we had only the annular detector available. So we were quite used to it for the studies of ultrathin sections with cytochemical reaction products. Up to now we have not met a situation in which the annular detector could not provide what the STEM-detector could. The contrast of both detectors can be inverted by a switch.

K Zierold: What is the advantage of the pseudo-colour pixel images?
Authors: There is not much gain from multi-pseudocoloured images beyond the point the human eye can appreciate better differences in colour than shades of grey. In the binary images black and white are as adequate. In the frequency histograms the colours are somewhat conflicting in the aim to differentiate the (three) sub-populations of grey values (see Figs. 6 and 9).

HK Hagler: I think the authors should substitute the word correlate for the word "integrate" throughout the paper.
Authors: We prefer to reserve the word correlation for the topographic relation of two elements. The term integration is used to underline that the measured electron scattering is composed as the sum of the elemental concentrations per pixel point within the delineated area. We agree that in the example chosen only one detectable element, platinum, is present. When more than one element is co-localized in the same pixel point, as shown elsewhere [14], this point can be made clearer.

HK Hagler: How have the various spot sizes been calibrated and how reliable are the numbers with changes in beam current?
Authors: The various spot sizes are not calibrated, the values given are the scale readings. So the conversion into counts/point/nm^2 suffers from the possible inaccuracy between scale reading and actual spot size. The net-intensity ratio between two spot sizes is rather constant, but does not include the mathematically predicted increase or decrease exactly. The variation in numbers with changes in beam current, measured directly at the insulated condenser-2 aperture, is shown in Figs. 18-19 and Table 4. In Fig. 18, the beam intensity was varied between typically 0.005 and 1.100 A upwards and downwards. It shows a straight line (R^2 = 0.9939 and 0.9931) for the $Pt_{M\alpha}$ and $Pt_{L\alpha}$ respectively, which values are somewhat improved for the correlation between P-b/b, 0.9983 and 0.9978. The lines go rather nicely through the origin. Similar observation can be obtained for the main values of the 256 points inside the reduced scan area analysis of these standards. The variation among the 256 points within the reduced scan area can be estimated from Fig. 19. The iron standard-derived R_x value does show a rather straight line, though not completely horizontal. Standard deviations are shown elsewhere [12].

Additional references

75. Roomans GM. (1980a) Problems in quantitative X-ray microanalysis of biological specimens. Scanning Electron Microsc. 1980; II: 309-320.
76. Roomans GM. (1980b) Quantitative X-ray microanalysis of thin sections, in X-ray Microanalysis in Biology (MA Hayat, ed.), University Park Press, Baltimore, 401-453.
77. Roomans GM, Kuypers GAJ. (1980) Background determination in quantitative X-ray microanalysis of biological thin sections. Ultramicroscopy, 5, 81-83.
78. de Bruijn WC, van Miert MPC. (1988) Extraneous background correction program for matrix-bound multiple point analyses. Scanning Microscopy, 2, to be published.

Please see page 1666 for legends to figures on the color plate at page 1667.

Fig. 5 Digitalized electron image of the reduced scan area indicated by the white square in Fig. 3. Unmanipulated colour monitor (CM) image.
Fig. 6 Frequency-histogram of the pixel points collected in Fig. 5. The original grey-value distribution-scale is shown. The three Gaussian-shaped sub-populations can be observed. The area from one grey-value population indicated by the cursor (white line) is given at the bottom (3.91%). CM-image.
Fig. 7 Partially binary image. The pixel points with grey values belonging to the resin are made monochromic, the grey values inside the cell maintain their sub-division in which grey-value intervals are converted in colours. Manipulated CM-image.
Fig. 8 True binary image in which at the same threshold as chosen in Fig. 7, now all intra-cellular grey-level values are also made monochromic. The area occupied by the cytoplasm can be calculated from the percentage of pixel points occupied by the cytoplasm. Manipulated CM-image.
Fig. 9 Frequency histogram of the picture shown in Fig. 7. The area of one grey-level value class selected (= epon) is indicated at the bottom (25.25%). Unmanipulated CM-image.
Fig. 10 Binary image showing the highest electron values, comprising the grey-level value in the highest classes, at the right hand side of the frequency histogram. Manipulated CM-image.
Fig. 11 Electron image of granule nr 1, obtained by reduction of the scan area to enclose only this single granule. (see Fig. 3). The image was obtained at 16 x 16 pixel points. The grey-level values are again converted in colours. Binary image: the cytoplasm and granule are monochromic. The threshold chosen to separate the cytoplasm from the granule is 166 c/p/s., which is identical with the threshold chosen in Fig. 10. Manipulated CM-image.
Fig. 12 Frequency histogram of the image shown in Fig. 11, at threshold 166 c/p/s. Manipulated CM-image.
Fig. 13 Platinum net-intensity distribution of granule 1. The (X-ray) threshold value that separates the granule Pt net-intensity best from the cytoplasmic Pt net-intensity values is 20 c/p/s. The way this value is objectively determined is calculated in Fig. 17. Manipulated CM-image.

5

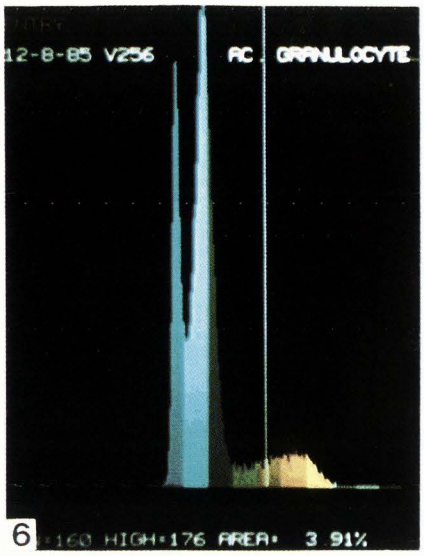

6

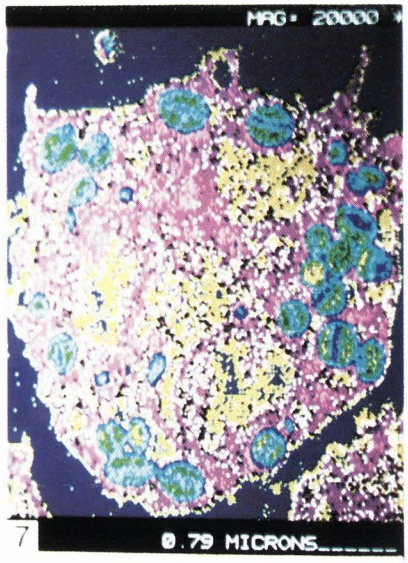

7

8

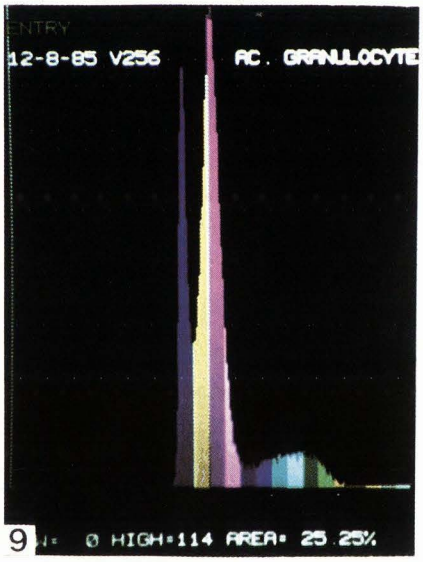

9

10

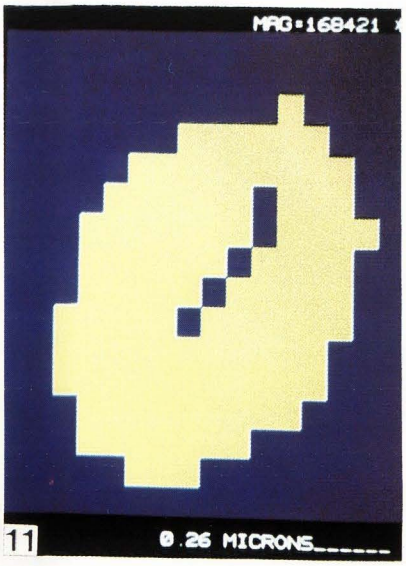

11

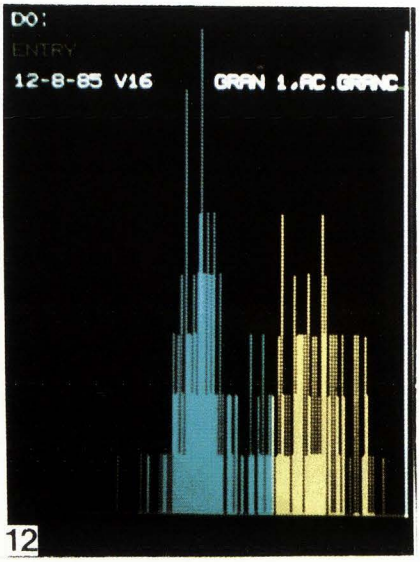

12

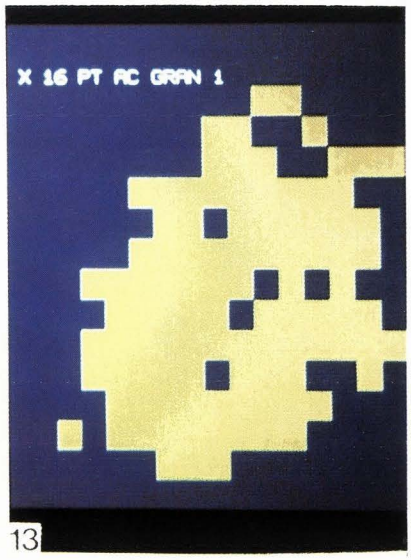

13